

¹ **neonSoilFlux: An R Package for Continuous
2 Sensor-Based Estimation of Soil CO₂ Fluxes**

³ John Zobitz¹ Edward Ayres² Zoey Werbin³ Ridwan Abdi¹
⁴ Natalie Ashburner-Wright⁴ Lillian Brown⁴
⁵ Ryan Frink-Sobierajski⁴ Lajntxiag Lee¹ Dijonë Mehmeti¹
⁶ Christina Tran⁴ Ly Xiong¹ Naupaka Zimmerman^{4,5}

⁷ ¹ Augsburg University, 2211 Riverside Avenue, Minneapolis, MN 55454

⁸ ² National Ecological Observatory Network, Battelle, 1685 38th Street, Suite 100, Boulder, CO
⁹ 80301

¹⁰ ³ Boston University, 5 Cummington Street, Boston, MA 02215

¹¹ ⁴ University of San Francisco, 2130 Fulton Street, San Francisco, CA 94117

¹² ⁵ University of Kansas, 1450 Jayhawk Boulevard, Lawrence, KS 66045

¹³ **Acknowledgments**

¹⁴ JZ—John Zobitz acknowledges Kathleen O'Rourke for code development. NZ—Naupaka

¹⁵ Zimmerman thanks technical staff at USF for support with field gear assembly and shipping.

¹⁶ We thank the NEON field staff and assignable assets teams for facilitating each of the six

17 NEON site visits. We are grateful to LI-COR technical staff for helpful discussions about
18 optimal soil chamber sampling methods. This work was supported by NSF DEB grant
19 #2017829 awarded to JZJohn Zobitz, and NSF DEB grant #2017860 awarded to NZNaupaka
20 Zimmerman. This material is based in part upon work supported by the National Ecological
21 Observatory Network (NEON), a program sponsored by the U.S. National Science Foundation
22 (NSF) and operated under cooperative agreement by Battelle. We also thank the reviewers
23 and subject editor for their constructive feedback.

24 **Conflict of Interest Statements**

25 None of the authors have a financial, personal, or professional conflict of interest related to this
26 work.

27 **Author Contributions**

28 Conceptualization: JZ, NZJohn Zobitz, Naupaka Zimmerman; Methodology: EA, JZ,
29 NZEdward Ayres, John Zobitz, Naupaka Zimmerman; Software: JZ, NZ, ZW, E A, DM,
30 RA, LX, LLJohn Zobitz, Naupaka Zimmerman, Zoey Werbin, Edward Ayres, Dijonë
31 Mehmeti, Ridwan Abdi, Ly Xiong, Lajntxiag Lee; Validation: JZ, NZJohn Zobitz, Naupaka
32 Zimmerman; Formal Analysis: JZ, NZ, DM, RA, LX, LLJohn Zobitz, Naupaka Zimmerman,
33 Dijonë Mehmeti, Ridwan Abdi, Ly Xiong, Lajntxiag Lee; Investigation: JZ, NZ, RF-S,
34 CT, NA-W, LBJohn Zobitz, Naupaka Zimmerman, Ryan Frink-Sobierajski, Christina
35 Tran, Natalie Ashburner-Wright, Lillian Brown; Resources: JZ, NZJohn Zobitz, Naupaka
36 Zimmerman; Data curation: JZ, NZ, DM, LXJohn Zobitz, Naupaka Zimmerman, Dijonë

³⁷ Mehmeti, Ly Xiong; Writing – original draft: JZ, NZ John Zobitz, Naupaka Zimmerman; Writ-
³⁸ ing – review and editing: JZ, NZ, ZW, EA, CT, DM, LX, John Zobitz, Naupaka Zimmerman,
³⁹ Zoey Werbin, Edward Ayres, Christina Tran, Dijoné Mehmeti, Ly Xiong; Visualization: JZ,
⁴⁰ NZ, DM, RA, LX, John Zobitz, Naupaka Zimmerman, Dijoné Mehmeti, Ridwan Abdi, Ly
⁴¹ Xiong; Supervision: JZ, NZ, John Zobitz, Naupaka Zimmerman; Project Administration: JZ;
⁴² NZ, John Zobitz, Naupaka Zimmerman; Funding Acquisition: JZ, NZ, John Zobitz, Naupaka
⁴³ Zimmerman.

⁴⁴ Data Availability

⁴⁵ Anonymous field-collected data, `neonSoilFlux` calculated outputs, and manuscript-generating
⁴⁶ code for peer review are provided as supplemental files. An anonymous link for peer-review is
⁴⁷ here: <https://doi.org/10.5281/zenodo.1695117>. This will be made publicly available upon
⁴⁸ publication.

49 **1 Abstract**

- 50 1. Accurate quantification of soil carbon fluxes is essential to reduce uncertainty in estimates
51 of the terrestrial carbon sink. However, these fluxes vary over time and across ecosystem
52 types and so it can be difficult to estimate them accurately across large scales. The flux
53 gradient method estimates soil carbon fluxes using co-located measurements of soil CO₂
54 concentration, soil temperature, soil moisture, and other soil properties. The National
55 Ecological Observatory Network (NEON) provides such data across 20 ecoclimatic domains
56 spanning the continental U.S., Puerto Rico, Alaska, and Hawai‘i.
- 57 2. We present an R software package (`neonSoilFlux`) that acquires soil environmental data
58 to compute half-hourly soil carbon fluxes for each soil replicate plot at a given terrestrial
59 NEON site. To assess the computed fluxes, we visited six focal NEON sites and measured
60 soil carbon fluxes using a closed-dynamic chamber approach.
- 61 3. Outputs from the `neonSoilFlux` showed agreement with measured fluxes (R^2 between
62 measured and `neonSoilFlux` outputs ranging from 0.04 to 0.81 depending on calculation
63 method used); measured outputs generally fell within the range of calculated uncertainties
64 from the gradient method. Calculated fluxes from `neonSoilFlux` aggregated to the daily
65 scale exhibited expected site-specific seasonal patterns.
- 66 4. While the flux gradient method is broadly effective, its accuracy is highly sensitive
67 to site-specific inputs, including the extent to which gap-filling techniques are used to
68 interpolate missing sensor data and to estimates of soil diffusivity and moisture content.
69 Future refinement and validation of `neonSoilFlux` outputs can contribute to existing
70 databases of soil carbon flux measurements, providing near real-time estimates of a critical
71 component of the terrestrial carbon cycle.

⁷² **1.1 Keywords**

⁷³ Soil carbon, carbon dioxide, flux gradient, carbon cycle, field validation, soil respiration,
⁷⁴ ecosystem variability, diffusion

⁷⁵ **2 Data for peer review**

⁷⁶ Anonymous field-collected data, `neonSoilFlux` calculated outputs, and manuscript-generating
⁷⁷ code for peer review are provided as supplemental files. An anonymous link for peer-review is
⁷⁸ here: <https://doi.org/10.5281/zenodo.16951117>. This will be made publicly available upon
⁷⁹ publication.

⁸⁰ **3 Introduction**

⁸¹ Soils contain the planet's largest reservoir of terrestrial carbon (Jobbágy & Jackson, 2000). A
⁸² critical component of this reservoir is soil organic matter, the accumulation of which is influenced
⁸³ by biotic factors such as above-ground plant inputs (Jackson et al., 2017). These inputs in
⁸⁴ turn are influenced by environmental factors such as growing season length, temperature, and
⁸⁵ moisture (Desai et al., 2022), which also affect the breakdown of soil organic matter and its
⁸⁶ return to the atmosphere. Across heterogeneous terrestrial landscapes, the interplay between
⁸⁷ these biotic and abiotic factors influence the size of the soil contribution to the terrestrial
⁸⁸ carbon sink (Friedlingstein et al., 2025). However, the heterogeneity of these processes across
⁸⁹ diverse ecosystems in the context of rapid environmental change leads to large uncertainty
⁹⁰ about the magnitude of this sink in the future, and thus there remains a pressing need to
⁹¹ quantify changes in soil carbon pools and fluxes across scales.

92 Ecological observation networks such as the United States' National Ecological Observatory
93 Network (NEON) and others (e.g. the globally-distributed FLUXNET or the European Inte-
94 grated Carbon Observation System) present a significant advancement in the nearly continuous
95 observation of biogeochemical processes at the continental scale. Notably, at 47 terrestrial
96 sites across the continental United States that span 20 ecoclimatic domains, NEON provides
97 half-hourly measurements of soil CO₂ concentration, temperature, and moisture at different
98 vertical depths. Each of these NEON sites also encompasses measurements of the cumulative
99 sum of all ecosystem carbon fluxes in an airshed using the eddy covariance technique (Baldocchi,
100 2014). Soil observations provided by NEON are on the same timescale and standardized with
101 eddy covariance measurements from FLUXNET. These types of nearly continuous observational
102 data (NEON and FLUXNET) can be used to reconcile differences between model-derived
103 or data-estimated components of ecosystem carbon flux (Jian et al., 2022; Luo et al., 2011;
104 Phillips et al., 2017; J. Shao et al., 2015; P. Shao et al., 2013; Sihi et al., 2016).

105 Estimated or observed soil carbon fluxes are a key metric for understanding change in soil
106 carbon pools over time (Bond-Lamberty et al., 2024). A soil carbon flux to the atmosphere (F_S ,
107 units $\mu\text{mol m}^{-2} \text{s}^{-1}$), represents the aggregate process of transfer of soil CO₂ to the atmosphere
108 from physical and biological processes (e.g. diffusion and respiration). Soil carbon fluxes can
109 be assumed to encompass soil carbon respiration from autotrophic or heterotrophic sources
110 (Davidson et al., 2006) and modeled with a exponential Q_{10} paradigm (Bond-Lamberty et al.,
111 2004; Chen & Tian, 2005; Hamdi et al., 2013).

112 One common method by which F_S is measured in the field is through the use of soil chambers
113 in a closed, well-mixed system (Norman et al., 1997) with headspace trace gas concentrations
114 measured with an infrared gas analyzer (IRGA). F_S can also be estimated from soil CO₂
115 measurements at different depths in the soil using the flux-gradient method (Maier & Schack-
116 Kirchner, 2014). Closed-chamber IRGA measurements, while being the most common method,

117 require either frequent in-person site visits or expensive and fragile automated systems. The
118 potential of the gradient method is that fluxes can be estimated from continuous data recorded
119 by robust solid-state sensors. The flux-gradient method is an approach that uses conservation of
120 mass to calculate flux at a vertical soil depth z at steady state by applying Fick's law of diffusion.
121 A simplifying assumption for the flux-gradient method is that there is no mass transfer in the
122 other spatial dimensions x and y (Maier & Schack-Kirchner, 2014). The diffusivity profile, a
123 key component of this calculation, varies across the soil depth as a function of soil temperature,
124 soil volumetric water content, atmospheric air pressure, and soil bulk density (Millington &
125 Shearer, 1971; Moldrup et al., 1999; Sallam et al., 1984).

126 Databases such as the Soil Respiration Database (SRDB) or the Continuous Soil Respiration
127 Database (COSORE) add to the growing network of resources for making collected observations
128 of soil fluxes available to other researchers (Bond-Lamberty, 2018; Bond-Lamberty et al., 2020;
129 Bond-Lamberty & Thomson, 2010; Jian et al., 2021; Jiang et al., 2024). However, these
130 databases currently encompass primarily direct soil measurements of fluxes (i.e. those using
131 methods like the closed-chamber method described above). Currently, NEON provides all
132 measurements to calculate F_S from Fick's law, but soil flux as a derived data product was
133 descoped from the initial network launch due to budget constraints (Berenbaum et al., 2015).
134 Deriving estimates of F_S using continuous sensor data across NEON sites [using NEON data](#)
135 thus remains a high priority.

136 This study describes an R software package, `neonSoilFlux`, that computes a standardized
137 estimate of F_S at all terrestrial NEON sites using the flux-gradient method. Using direct
138 chamber-based field observations of soil carbon dioxide flux from a subset of terrestrial NEON
139 sites spanning six states, we provide a direct validation of F_S from `neonSoilFlux`. [While](#)
140 [open source R software tools currently exist for processing chamber-based flux measurements](#)
141 [\(Jurasinski et al., 2022; Pedersen, 2024; Rheault et al., 2024; Wilson et al., 2024; Zhao, 2019\)](#).

¹⁴² to our knowledge this is the first package that incorporates NEON data directly.

¹⁴³ Key objectives of this study are to:

- ¹⁴⁴ 1. Apply the flux-gradient method to estimate soil CO₂ flux from continuous sensor mea-
- ¹⁴⁵ surements across six NEON sites.
- ¹⁴⁶ 2. Benchmark estimated soil carbon fluxes against field measurements (e.g. direct chamber
- ¹⁴⁷ measurements of soil flux).
- ¹⁴⁸ 3. Identify sources of error in the flux-gradient approach across diverse sites in order to
- ¹⁴⁹ guide future work.

¹⁵⁰ **4 Materials and Methods**

¹⁵¹ **4.1 Field methods**

¹⁵² **4.1.1 Focal NEON Sites**

¹⁵³ In order to acquire field data to validate model predictions of flux, we selected six terrestrial
¹⁵⁴ NEON sites for analysis. We conducted roughly week-long field measurement campaigns at
¹⁵⁵ these sites, which span a range of environmental gradients and terrestrial domains (Table 1).
¹⁵⁶ SJER, SRER, and WREF were visited during May and June of 2022, and WOOD, KONZ,
¹⁵⁷ and UNDE during May and June of 2024.

¹⁵⁸ **4.1.2 Soil collar placement**

¹⁵⁹ Either one (2022 sampling campaign) or two (2024 sampling campaign) PVC soil collars (20.1
¹⁶⁰ cm inside diameter) were installed in close proximity to the permanent NEON soil sensors at

161 each site (Figure 1). As instruments in the NEON soil sensor arrays can occasionally break
162 down or stop working, the specific soil plot where we made measurements was chosen at each
163 site in consultation with NEON staff to maximize likelihood of quality soil sensor measurements
164 during the duration of the IRGA measurements. The plot selected at each site (out of the 5 in
165 each replicate array at each site) are presented in the last column of Table 1. After installation,
166 collar(s) were left to equilibrate for approximately 24 hours prior to any measurements being
167 taken.

168 **4.1.3 Infrared gas analyzer measurements of soil CO₂ flux**

169 In 2022, we then made measurements of flux on an hourly interval for 8 hours each day.
170 Measurements were taken from roughly 8 am to 4 pm, with the time interval selected to
171 capture the majority of the diurnal gradient of soil temperature each day. These measurements
172 were made using a LI-6800 infrared gas analyzer instrument (LI-COR Environmental, Lincoln,
173 NE) fitted with a soil chamber attachment (attachment 6800-09). In 2024, we again used the
174 same LI-6800 instrument, but made half-hourly measurements over an approximately 8 hour
175 period. In addition, in 2024 we also installed a second collar and used a second instrument, an
176 LI-870 CO₂ IRGA, connected to an automated robotic chamber (LI-COR chamber 8200-104)
177 controlled by an LI-8250 multiplexer to make automated measurements. The multiplexer was
178 configured to take half-hourly measurements 24 hours a day for the duration of our sampling
179 bout at each site. Each instrument was paired with a soil temperature and moisture probe
180 (Stevens HydraProbe, Stevens Water, Portland, OR) that was used to make soil temperature
181 and moisture measurements concurrent with the CO₂ flux measurements. Chamber volumes
182 were set by measuring collar offsets at each site. System checks were conducted daily for the
183 LI-6800 and weekly for the LI-8250. Instruments were factory calibrated before each field
184 season.

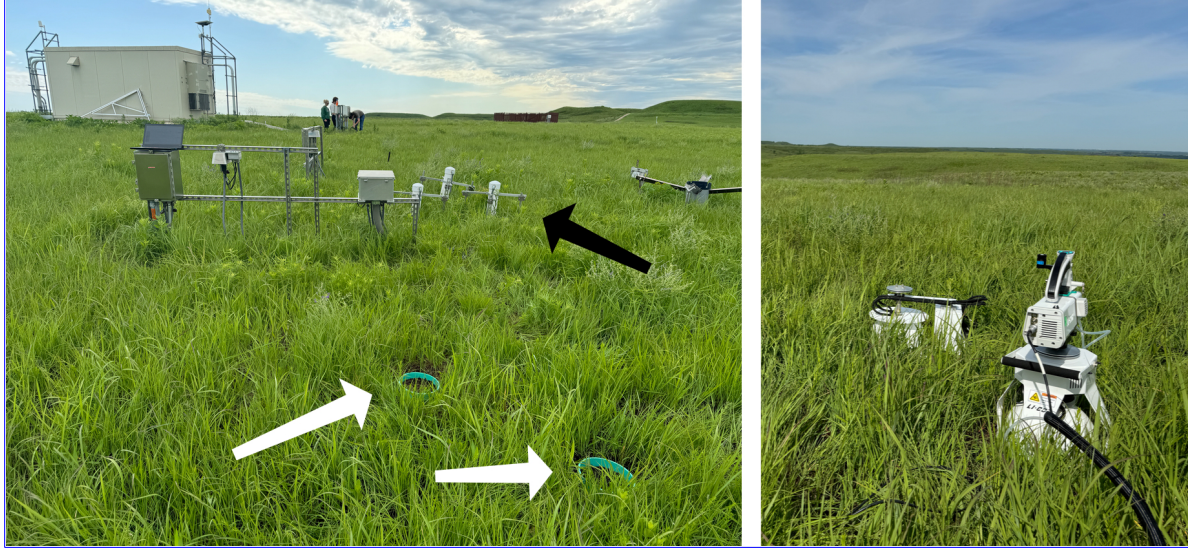


Figure 1: Spatial layout of field sampling using a closed-dynamic chamber setup at a representative NEON site (KONZ). Left image shows collars (white arrows) and permanent soil sensor installation (black arrow) and right image shows the LI-6800 (foreground) and LI-8200-104 (background) instruments placed on the collars.

g of NEON sites studied for field work and analysis. Site refers to NEON site : Santa Rita Experimental Range (SRER), San Joaquin Experimental Range (SJER), Wind River Experimental Forest (WREF), Chase Lake National Wildlife Refuge (WOOD), Konza Prairie Biological Station (KONZ), and the University of Notre Dame Environmental Research Center (UNDE). Location is reported in decimal degrees of latitude and longitude. Other abbreviations include Mean Annual Temperature (MAT); \bar{T}_S : average soil temperature during field measurements; \overline{SWC} : average soil water content during field measurements. Dates refer to field measurement dates for each site. Plot refers to the particular location in the soil sensor array (labeled as HOR by NEON) where field measurements were made.

Site	Location	Ecosystem	MAT	\bar{T}_S	MAP	\overline{SWC}	Dates	Plot
SRER	31.91068, -110.83549	Shrubland	19.3 °C	47.6 °C	346 mm	4.0%	May 29– June 1 2022	004
SJER	37.10878, -119.73228	Oak woodland	16.4 °C	41.7 °C	540 mm	1.2%	June 1–4 2022	005
WREF	45.82049, -121.95191	Evergreen forest	9.2 °C	15.3 °C	2225 mm	27.2%	June 7–9 2022	001
WOOD	47.1282, -99.241334	Restored prairie	4.9 °C	14.9 °C	495 mm	14.9%	June 3–9 2024	001
KONZ	39.100774, -96.563075	Tallgrass prairie	12.4 °C	23.4 °C	870 mm	23.4%	May 29– June 1 2024	001

g of NEON sites studied for field work and analysis. Site refers to NEON site : Santa Rita Experimental Range (SRER), San Joaquin Experimental Range R), Wind River Experimental Forest (WREF), Chase Lake National Wildlife e (WOOD), Konza Prairie Biological Station (KONZ), and the University tre Dame Environmental Research Center (UNDE). Location is reported in al degrees of latitude and longitude. Other abbreviations include Mean Annual erature (MAT); \bar{T}_S : average soil temperature during field measurements; \bar{SWC} : ge soil water content during field measurements. Dates refer to field measurement for each site. Plot refers to the particular location in the soil sensor array ed as HOR by NEON) where field measurements were made.

Site	Location	Ecosystem	MAT	\bar{T}_S	MAP	\bar{SWC}	Dates	Plot
UNDE	46.23391, -89.537254	Deciduous forest	4.3 °C	13.0 °C	802 mm	13.0%	May 22–25 2024	004

185 4.1.4 Post-collection processing of field data

186 We used LI-COR SoilFluxPro software (v 5.3.1) to assess the data after collection and to
187 inform sampling parameters. We checked appropriateness of dead band and measurement
188 durations using built-in evaluation tools. Based on this, the deadband period was set for 30-40
189 seconds, depending on the site, and the measurement duration was 180 seconds with a 30
190 second pre-purge and a 30 second post-purge at most sites, and a 90 second pre- and post-purge
191 at sites with higher humidity due to recent precipitation events. We also assessed the R^2 of
192 linear and exponential model fits to measured CO₂ to verify measurement quality.

193 4.2 neonSoilFlux R package

194 We developed an R package called `neonSoilFlux` (Zobitz et al., 2024) to compute half-hourly
195 soil carbon fluxes and uncertainties from NEON data. The objective of the `neonSoilFlux`
196 package is a unified workflow (Figure 2) for soil data acquisition and analysis that supplements
197 the existing `neonUtilities` data acquisition R package (Lunch et al., 2025).

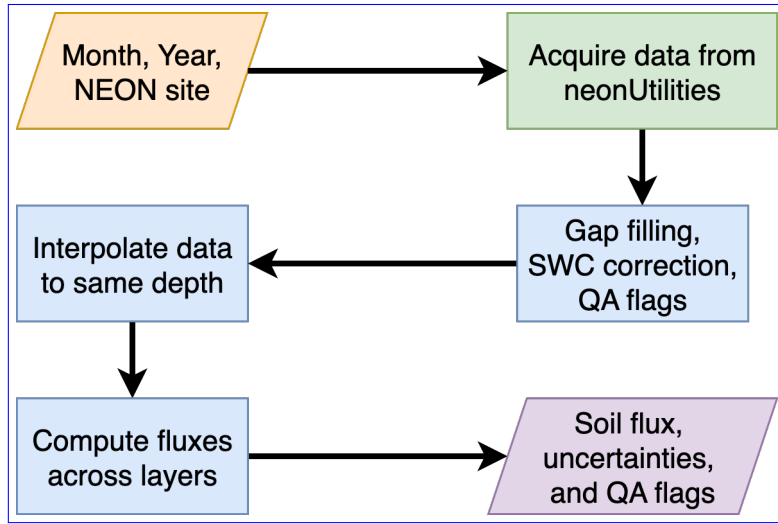


Figure 2: Diagram of `neonSoilFlux` R package. For a given month, year, and NEON site (orange parallelogram), the package acquires all relevant data to compute F_S using the `neonUtilities` R package (green rectangle). Data are gap-filled according to reported QA flags and adjusted for changes in soil water content (SWC) calibration coefficients, then interpolated to the same measurement depth before computing the soil flux, uncertainties, and final QA flags (blue rectangles). The package reports the associated soil flux, uncertainties, and quality assurance (QA) flags for the user (purple parallelogram).

198 At a given NEON site there are five replicate soil plots, each with measurements of soil
 199 CO₂ concentration, soil temperature, and soil moisture at different depths (Figure 3).
 200 The `neonSoilFlux` package acquires measured soil CO₂ concentration ([National Ecological Observatory Network \(NEON\) NEON](#), 2024b), soil temperature ([National Ecological Observatory Network \(NEON\) NEON](#), 2024d), soil water content ([National Ecological Observatory Network \(NEON\) NEON](#), 2024e), barometric pressure from the nearby tower ([National Ecological Observatory Network \(NEON\) NEON](#), 2024a), and soil properties (e.g. bulk density) ([National Ecological Observatory Network \(NEON\) NEON](#), 2024c) from a range of different NEON data products. The static soil properties were collected by NEON staff from a nearby soil pit during initial site characterization and are assumed to be constant at each site. A soil flux calculation is computed at each replicate soil plot.

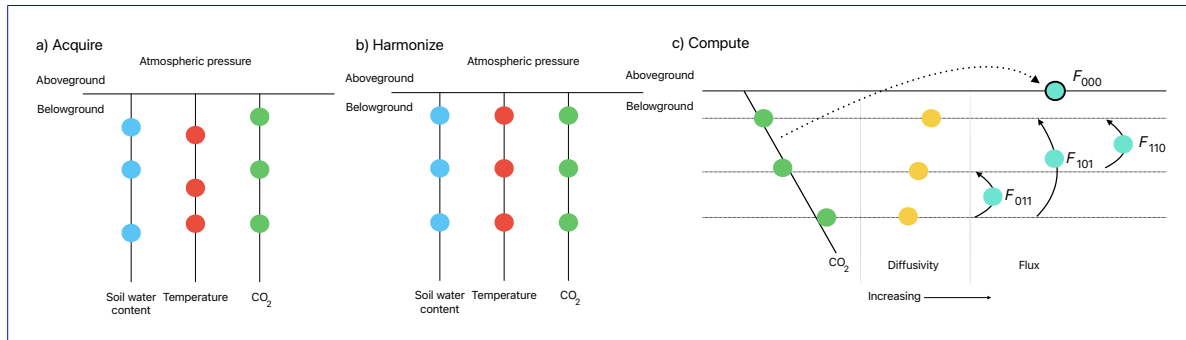


Figure 3: Model diagram of the data workflow for the `neonSoilFlux` R package. a) Acquire: Data are obtained for a given NEON location and horizontal sensor location, which includes soil water content, soil temperature, CO₂ concentration, and atmospheric pressure. All data are screened for quality assurance; if gap-filling of missing data occurs, it is flagged for the user. b) Harmonize: Any belowground data are then harmonized to the same depth as CO₂ concentrations using linear regression. c) Compute: The flux across a given depth is computed via Fick's law, denoted with F_{ijk} , where i , j , or k are either 0 or 1 denoting the layers the flux is computed across (i = closest to surface, k = deepest). F_{000} represents a flux estimate where the gradient dC/dz is the slope of a linear regression of CO₂ with depth.

209 The workflow to compute a value of F_S with `neonSoilFlux` consists of three primary steps,
 210 illustrated in Figure 3. First, NEON data are acquired for a given site and month via the

211 `neonUtilities` R package (yellow parallelogram and green rectangle in Figure 2 and Panel
212 a in Figure 3). Acquired environmental data can be exported to a comma separated value
213 file for additional analysis. Quality assurance (QA) flags are reported as an indicator variable.
214 Since the calibration coefficients on the soil water content sensors have changed over time
215 ([National Ecological Observatory Network \(NEON\)](#)[NEON](#), 2024e), raw sensor measurements
216 were back-calculated and soil-specific calibrations were applied following Ayres et al. (2024) to
217 generate a consistent time series at each measurement location.

218 The second step is harmonizing the data to compute soil fluxes across soil layers. This
219 step consists of three different actions (blue rectangles in Figure 2 and Panel b in Figure 3).
220 If a given observation by NEON is reported as not passing a quality assurance check, we
221 applied a gap filling method to replace that measurement with its monthly mean at that same
222 depth (Section 4.2.1). Belowground measurements of soil water and soil temperature are then
223 interpolated to the same depth as soil CO₂ measurements. The diffusivity (Section 4.2.2) and
224 soil flux across different soil layers (Section 4.2.3) are then computed.

225 The third and final step is computing a surface soil flux through extrapolation to the surface
226 (purple parallelogram in Figure 2 and Panel c in Figure 3). Uncertainty on a soil flux
227 measurement is computed through quadrature. An aggregate quality assurance (QA) flag for
228 each environmental measurement is also reported, representing if any gap-filled measurements
229 were used in the computation of a soil flux. Within the soil flux-gradient method, several
230 different approaches can be used to derive a surface flux (Maier & Schack-Kirchner, 2014); the
231 `neonSoilFlux` package reports four different possible values for soil surface flux (Section 4.2.3)
232 for each of two different methods of diffusivity estimation, for a total of eight estimates of
233 flux.

234 **4.2.1 Gap-filling routine**

235 NEON reports QA flags as binary values for each measurement and half-hourly interval. For a
236 given half-hour, if any input variable (soil CO₂ concentration, soil temperature, or soil moisture)
237 at depth z is flagged, computation of F_S is not possible. To address this, flagged measurements
238 and their uncertainties were replaced with a bootstrapped monthly mean (\bar{m}) and monthly
239 standard deviation (\bar{s}) (Efron & Tibshirani, 1994).

240 For each month, depth z , and variable, we computed bootstrapped estimates of \bar{m} and \bar{s}
241 from the vectors of unflagged measurements (\mathbf{m}), reported standard errors (σ), and the 95%
242 confidence interval (ϵ , or expanded uncertainty; Farrance & Frenkel (2012)). We also defined a
243 bias vector $\mathbf{b} = \sqrt{\epsilon^2 - \sigma^2}$, which quantifies the spread of uncertainty in a given period and is
244 incorporated into \bar{m} .

245 From these, 5000 bootstrap samples were generated for \mathbf{m} , σ , and \mathbf{b} . For each sample
246 (m_k, b_k, σ_k), we generated a vector \mathbf{n} (length $N = 5000$) by drawing from a normal distribution
247 with mean $m_k + b_k$ and standard deviation σ_k . The sample mean and standard deviation were
248 then computed from \mathbf{n} . The resulting distributions of sample means and sample standard
249 deviations provided the bootstrapped monthly mean (\bar{m}) and standard error (\bar{s}) respectively.

250 This gap-filling procedure provides a consistent treatment across all data streams. However,
251 alternative approaches may be better suited for longer gaps (e.g., correlations with other NEON
252 measurement levels or soil plots) or for variable-specific conditions. We discuss the effect of
253 gap-filling on our results in Section 6.1.

254 **4.2.2 Soil diffusivity**

255 Soil diffusivity D_a at a given measurement depth is the product of the diffusivity in free air
256 $D_{a,0}$ ($\text{m}^2 \text{ s}^{-1}$) and the tortuosity ξ (no units) (Millington & Shearer, 1971).

257 We compute $D_{a,0}$ with Equation 1:

$$D_{a,0} = 0.0000147 \cdot \left(\frac{T_i + 273.15}{293.15} \right)^{1.75} \cdot \left(\frac{P}{101.3} \right) \quad (1)$$

258 where T_i is soil temperature ($^\circ\text{C}$) at depth i (National Ecological Observatory Network
259 (NEON)NEON, 2024d) and P surface barometric pressure (kPa) (National Ecological
260 Observatory Network(NEON)NEON, 2024a).

261 Previous studies by Sallam et al. (1984) and Tang et al. (2003) demonstrated the sensitivity
262 of modeled F_S depending on the tortuosity model (ξ) used to compute diffusivity. At low
263 soil water content, the choice of tortuosity model can lead to order-of-magnitude differences
264 in D_a , which in turn affect modeled F_S . The neonSoilFlux package currently includes two
265 approaches to calculate ξ , representing the range of tortuosity behavior reported in Sallam et
266 al. (1984).

267 The first approach is the Millington-Quirk model (Millington & Shearer, 1971), in which
268 tortuosity depends on both porosity and soil water content:

$$\xi = \frac{(\phi - SWC_i)^{10/3}}{\phi^2} \quad (2)$$

269 In Equation 2, SWC is the soil water content at depth i (National Ecological Observatory
270 Network (NEON)NEON, 2024e) and ϕ is the porosity, which in turn is a function of soil
271 physical properties (National Ecological Observatory Network (NEON)NEON, 2024c):

$$\phi = \left(1 - \frac{\rho_s}{\rho_m}\right) (1 - f_V) \quad (3)$$

272 In Equation 3, ρ_m is the particle density of mineral soil (2.65 g cm^{-3}), ρ_s the soil bulk density (g
273 cm^{-3}) excluding coarse fragments greater than 2 mm (National Ecological Observatory Network
274 (NEON)NEON, 2024c), and f_V is a site-specific value that accounts for the proportion of
275 soil fragments between 2-20 mm. Soil fragments greater than 20 mm were not estimated due
276 to limitations in the amount of soil that can be analyzed (National Ecological Observatory
277 Network (NEON)NEON, 2024c). We assume that rock fragments contain no internal pores.

278 The Millington-Quirk model assumes ξ is modulated by the amount of fluid saturation in soil
279 pores (Millington & Shearer, 1971). In contrast, the Marshall model (Marshall, 1959) expresses
280 tortuosity as only a function of porosity ($\xi = \phi^{1.5}$), with ϕ defined from Equation 3. The
281 Marshall model is independent of soil water content and assumes tortuosity is only governed
282 by soil structure. The `neonSoilFlux` package allows users to choose the tortuosity model most
283 appropriate for site-specific conditions and research goals.

284 **4.2.3 Soil flux computation**

285 We applied Fick's law (Equation 4) to compute the soil flux F_{ij} ($\mu\text{mol m}^{-2} \text{s}^{-1}$) across two
286 soil depths i and j :

$$F_{ij} = -D_a \frac{dC}{dz} \quad (4)$$

287 where D_a is the diffusivity ($\text{m}^2 \text{ s}^{-1}$) and $\frac{dC}{dz}$ is the gradient of CO₂ molar concentration ($\mu\text{mol m}^{-3}$, so the gradient has units of $\mu\text{mol m}^{-3} \text{ m}^{-1}$). The soil surface flux is theoretically defined
288 by applying Equation 4 to measurements collected at the soil surface and directly below the
289 surface. Measurements of soil temperature, soil water content, and soil CO₂ molar concentration
290 across the soil profile allow for application of Equation 4 across different soil depths. Each
291 site had three measurement layers, so we denote the flux as a three-digit subscript F_{ijk} with
292 indicator variables i , j , and k indicate if a given layer was used (written in order of increasing
293 depth), according to the following:

- 295 • F_{000} is a surface flux estimate using the intercept of the linear regression of D_a with
296 depth and the slope from the linear regression of CO₂ with depth (which represents $\frac{dC}{dz}$
297 in Fick's Law). Tang et al. (2003) used this approach to compute fluxes in an oak-grass
298 savannah.
- 299 • F_{110} is a flux estimate across the two shallowest measurement layers.
- 300 • F_{011} is a flux estimate across the two deepest measurement layers.
- 301 • F_{101} is a flux estimate across the shallowest and deepest measurement layers.

302 For F_{110} , F_{011} , and F_{101} , the diffusivity used in Fick's Law is always at the deeper measurement
303 layer. When used as a surface flux estimate we assume CO₂ remains constant above this flux
304 depth. Uncertainty in all F_{ijk} values was quantified using quadrature (Taylor, 2022). These
305 computed fluxes could provide the basis for additional soil flux estimates. For example, Tang et
306 al. (2005) estimated surface flux by linearly extrapolating F_{110} and F_{011} to the soil surface.

307 4.3 Post processing evaluation

308 Following collection of field measurements and calculation of the soil fluxes from `neonSoilFlux`
309 package, we compared measured F_S based on closed-dynamic chamber measurements with the

Table 2: Summary of measured soil characteristics and flux results from field measurements across six NEON sites using a LI-COR 6800 (LI-870/8250 measurements omitted to enable direct comparability) via the closed-dynamic chamber method. Numeric values for soil CO₂ flux, soil temperature, and volumetric soil water content (VSWC) are the mean and standard deviation of field measurements at each site.

Site	Flux μmol m ⁻² s ⁻¹	Soil temp °C	VSWC cm ³ cm ⁻³	n
UNDE	2.55 ± 0.26	14.33 ± 0.77	0.33 ± 0.02	61
WOOD	3.02 ± 0.4	16.01 ± 1.54	0.28 ± 0.01	53
WREF	3.62 ± 0.3	15.34 ± 1.76	0.27 ± 0.06	21
KONZ	6.35 ± 0.97	27.28 ± 4.14	0.37 ± 0.01	44
SJER	0.94 ± 0.02	41.68 ± 11.22	0.01 ± 0.01	32
SRER	0.72 ± 0.09	47.64 ± 7.46	0.04 ± 0.01	32

310 LI-COR instruments to a given soil flux calculation from `neonSoilFlux` for each site and flux
 311 computation method and quantified the relationship statistically (R^2). Finally, for a half-hourly
 312 interval we also computed a *post hoc* diffusivity (D_a) using the LI-COR flux along with the
 313 CO₂ surface gradient reported by NEON using the measurement levels closest to the surface.

314 5 Results

315 5.1 Concordance between modelled and measured soil CO₂ flux

316 The sites we visited ranged substantially in both their annual average temperature and
 317 precipitation as well as their biome type (Table 2). These differences also influenced the wide
 318 range of observed flux rates across sites.

319 The timeseries of the measured fluxes from the LI-COR 6800 and 870/8250 were compared
 320 to modeled soil fluxes from the `neonSoilFlux` R package (Figure 4). We also assessed year-
 321 long estimated flux time series and compared those to field measurements made at each site
 322 (Figure 5). Results are reported in local time. Where applicable, sites are displayed from left

323 to right by increasing soil temperature (Table 1). Positive values of the flux indicate that there
 324 is a flux moving towards the surface. Overall, with the exception of SRER (discussed later) the
 325 computed fluxes determined using a variety of plausible methods spanned the field-measured
 326 fluxes, but the specific flux-gradient method that best approximated field measurements varied
 327 by site.

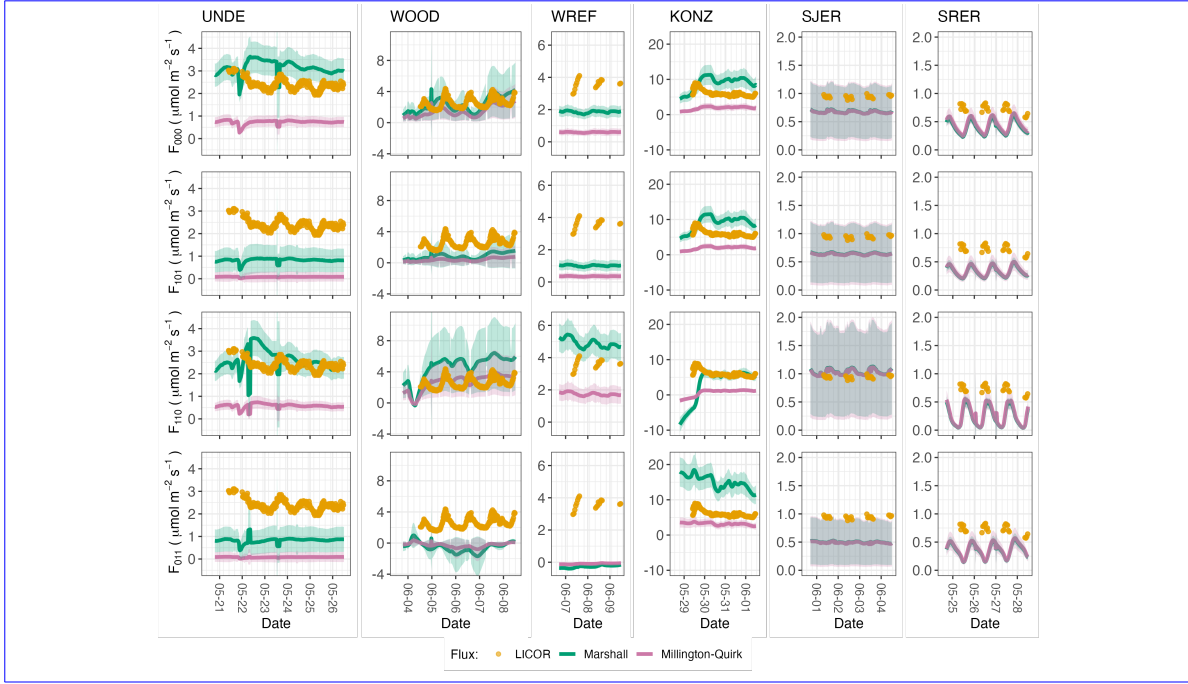


Figure 4: Timeseries of soil surface flux (F_S) from field-measured (yellow lines) and modeled soil fluxes (green or purple lines) by the `neonSoilFlux` R package. Fluxes from the `neonSoilFlux` R package are separated by the diffusivity model used (Millington-Quirk or Marshall, Section 4.2.2). Individual vertical axis labels in the first column represent the measurement levels where the flux-gradient approach is applied (Section 4.2.3). Ribbons for modeled soil fluxes represent ± 1 standard deviation. Results are reported in local time. WREF, SJER, and SRER were sampled in 2022, and UNDE, WOOD, and KONZ were sampled in 2024. Sites (columns) are arranged from left to right in terms of increasing mean annual temperature.

328 We calculated a statistical relationship between the various estimates of soil flux computed by
 329 `neonSoilFlux` and the field-measured fluxes within daily interval periods. Statistics for these
 330 comparisons are reported in Figure 6, which also shows how these fall relative to a 1:1 line.

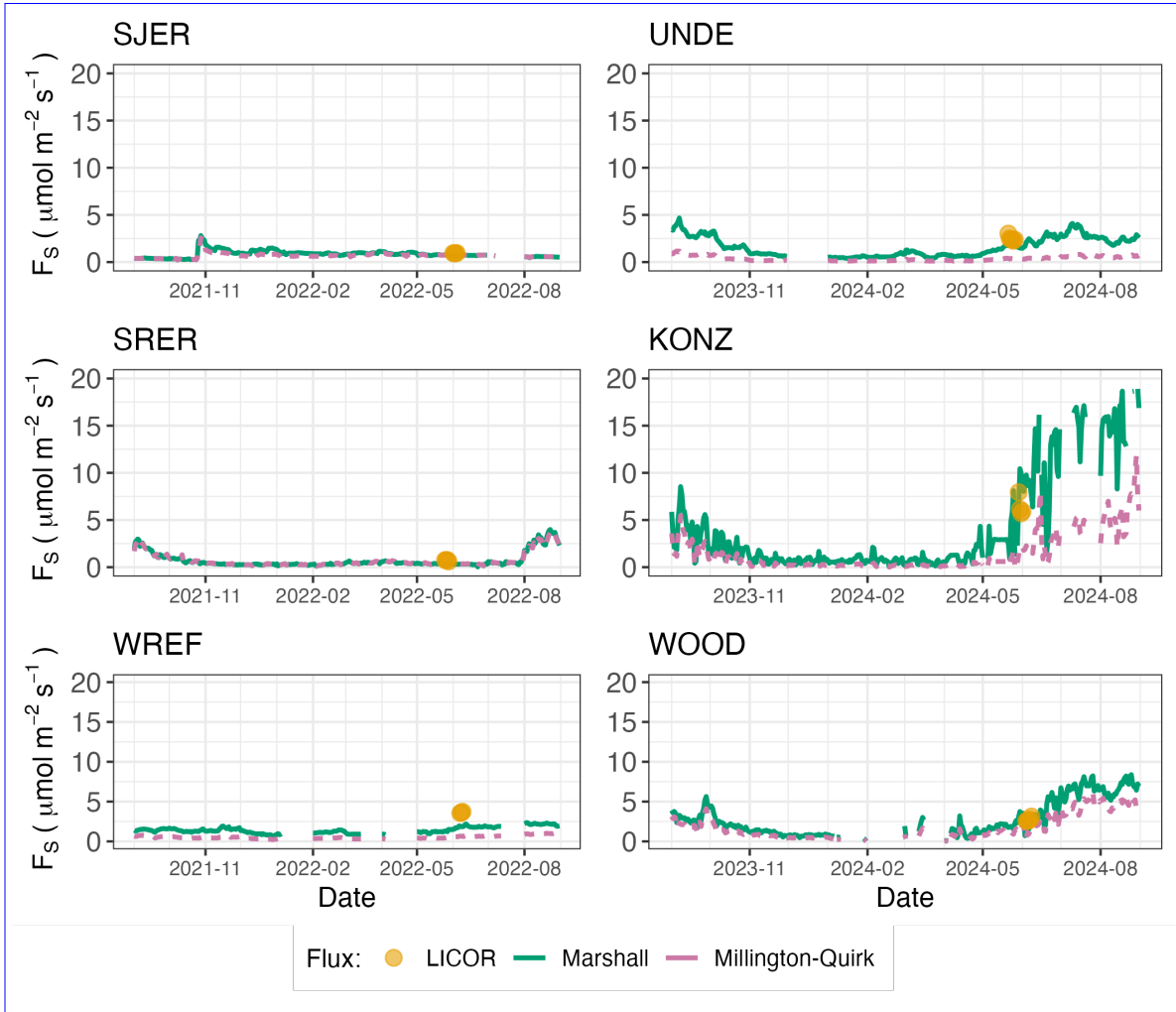


Figure 5: Timeseries of both daily-averaged field F_S (yellow circles) and daily ensemble averaged soil fluxes (average of F_{000} , F_{101} , F_{011} , F_{110} , Section 4.2.3) by the `neonSoilFlux` R package, separated by the diffusivity model used (green or purple lines, Millington-Quirk or Marshall, Section 4.2.2).

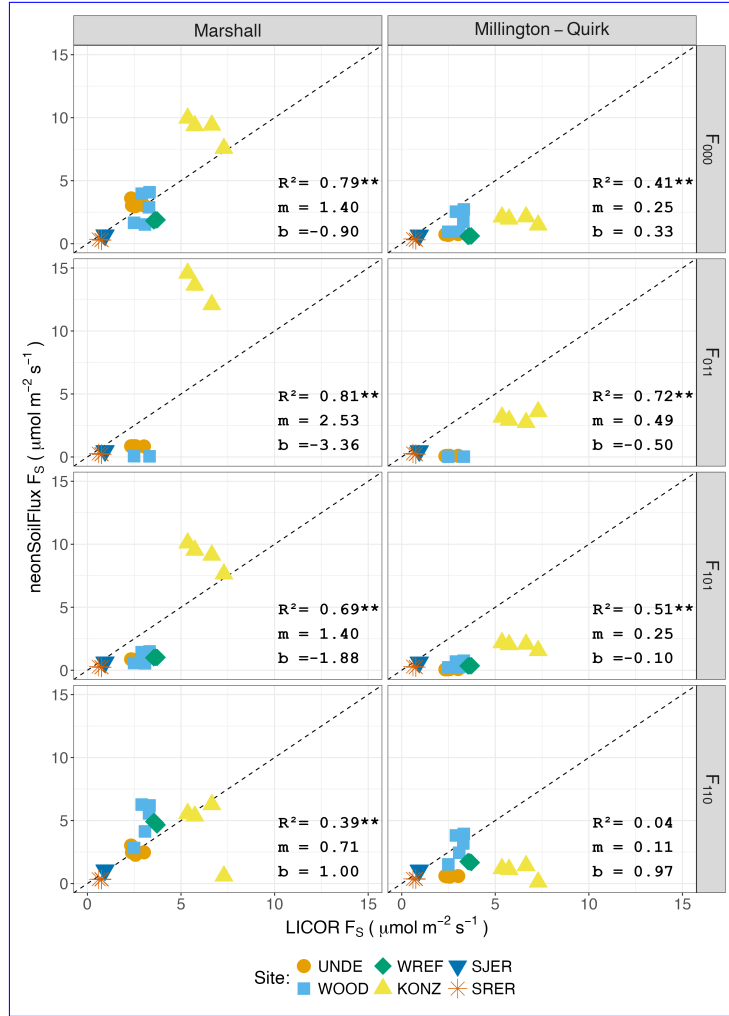


Figure 6: Statistical comparison between measured fluxes at each NEON site with fluxes reported by `neonSoilFlux` with the different flux calculation approaches and diffusivity calculations applied. Points are daily averages and LICOR F_S values are from the 6800 instrument only, for consistency. The dotted line represents a 1:1 relationship, and the reported R^2 quantifies the relationship between field-measured and `neonSoilFlux` estimated fluxes. * = significance at the 5% level, ** = significance at the 1% level. The [slope \(\$m\$ \) and intercept \(\$b\$ \) of the linear regression between measured and modeled fluxes are also reported](#). The low-value outlier from KONZ in the F_{110} Marshall plot is an example of the effect of inverted CO₂ gradients causing an estimated flux to be negative, bringing down the daily mean, which later resolved as the soils dried back out.

331 5.2 Effects of method choice on diffusivity estimates

332 In four of six field sites, the *post hoc* D_a estimate fell roughly between the two diffusion
333 estimation methods; however this was less the case in the two driest sites, SJER and SRER
334 (Table 1), where the field estimate of diffusivity was either lower or higher than both of the
335 other methods (Figure 7).

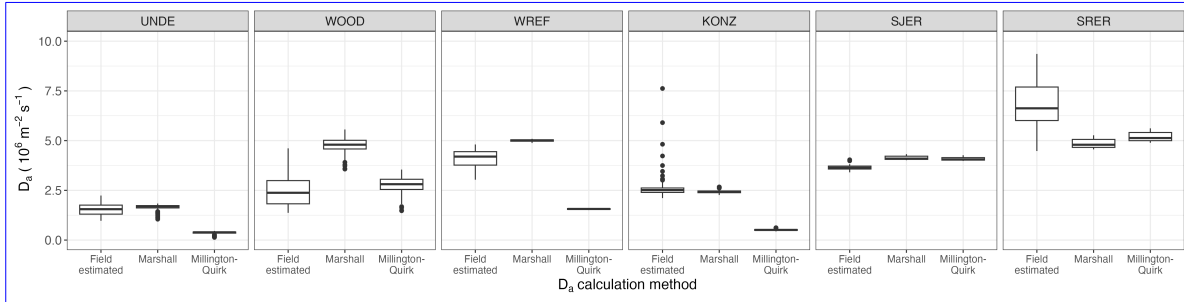


Figure 7: Distribution of diffusivity (D_a) at each study site. Values of D_a were provided by the `neonSoilFlux` package, computed from the Millington-Quirk or Marshall models (Section 4.2.2). A post-hoc estimate of diffusivity (labeled as “Field estimated”) was computed through the field measured flux (Figure 4), divided by the CO₂ gradient from the measurement levels closest to the soil surface, as reported by NEON. We only used F_S measured by the LICOR 6800 at all sites to standardize comparisons.

336 6 Discussion

337 This study presents a unified data science workflow to efficiently process automated measure-
338 ments of belowground soil CO₂ concentrations, soil water content, and soil temperature to
339 infer estimates of soil surface CO₂ effluxes through application of Fick’s Law (Equation 4).
340 Our core goals in this study were: (1) to generate estimates of soil flux from continuous soil
341 sensor data at terrestrial NEON sites using the flux-gradient method and then (2) to compare
342 those estimates to field-measured fluxes based on the closed chamber approach at six NEON
343 focal sites. We discuss our progress toward these core goals through (1) an overall evaluation

344 of the flux-gradient approach (and uncertainty calculation) and (2) site-specific evaluation of
345 differences in estimated vs measured fluxes.

346 **6.1 General evaluation of flux-gradient approach**

347 Key assumptions of the flux-gradient approach are that CO₂ concentrations increase throughout
348 the soil profile such that the highest concentrations are observed in the deepest layers. Addition-
349 ally, field flux measurements should correlate with F_{000} because they represent surface fluxes.
350 Periods where this gradient condition are not met generally are connected to processes that occur
351 during soil wetting events, where more shallow soil layers produce higher concentrations of CO₂
352 due to microbial respiration pulses following rewetting. This effect is likely to be largest at sites
353 with rich organic soils (e.g. KONZ). Based on this reasoning, in these types of situations we would
354 *a priori* expect F_{011} (deepest layers) $\leq F_{101} \leq F_{110}$ (shallow layers) $\leq F_{000}$ (all layers) be-
355 cause the previous flux estimates rely primarily on CO₂ concentrations at deeper depths, and
356 could miss high concentrations of CO₂ produced in shallower layers.

357 When modeling soil respiration, typically a non-linear response function that also considers soil
358 type is used (Bouma & Bryla, 2000; Yan et al., 2016, 2018). For the `neonSoilFlux` package,
359 soil type is connected to the measurement of bulk density, which was characterized at each
360 NEON site. This bulk density estimate is based on replicate samples collected from the site
361 megapit at a subset of soil horizons, with an estimated uncertainty of $\pm 5\%$ ([National Ecological
362 Observatory Network \(NEON\)](#)[NEON](#), 2024c). Coarse fragment estimates also have very large
363 uncertainties, but because the volume fraction tends to be low in surface soils it is unlikely to
364 contribute much additional flux uncertainty.

365 Our results suggest that the most important way to improve reliability of the flux estimate is
366 to reduce the usage of gap-filled data. The current approach to gap filling in `neonSoilFlux`

uses monthly mean data to gap fill—this approach decreases the ability of the estimate to be responsive to short-term pulses that occur with rapid weather shifts. Four sites (KONZ, SRER, WREF, and UNDE) had more than 75% of half-hourly periods with no-gap filled measurements (Figure S1, Supplementary Information). Two sites (SJER and WOOD) had more than 75% of half-hourly intervals with just one gap-filled measurement. The large uncertainty evident in Figure 4 for estimates from WOOD and SJER are thus due in part to the gap-filling used in these sites (Figure S1). While we did not need to use gap-filled measurements to compute the flux at WREF, field data collection occurred following a severe rainstorm, with soils at the beginning of the sampling week near their water holding capacity. In general, we recommend that whenever possible, knowledge of local field conditions should influence analysis decisions in addition to any QA filtering protocols in the `neonSoilFlux` package.

We recognize that this gap-filling approach may lead to gap-filled values that are quite different from the actual values, such as an underestimate of soil moisture following rain events. Further extensions of the gap filling method could use more sophisticated gap-filling routines, similar to what is used for net ecosystem carbon exchange (Falge et al., 2001; Liu et al., 2023; Mariethoz et al., 2015; Moffat et al., 2007; Zhang et al., 2023). Additionally, since the deepest temperature and soil moisture sensors are located below the deepest CO₂ sensors at NEON sites, it is possible that excluding these deeper layers from consideration prior to analysis would lead to a reduced need for gap filling. Future iterations of the `neonSoilFlux` package may incorporate this as an option. The current gap-filling routine provides a consistent approach that can be applied to each data stream, but further work may explore alternative gap-filling approaches.

6.2 Evaluation of flux-gradient approach at each site

Derived results from the `neonSoilFlux` package have patterns that are broadly consistent with those directly measured in the field (Figure 4 and Figure 5), even though statistical comparisons

391 between the field-measured and `neonSoilFlux` values were quite variable (e.g. R^2 ranging
392 from 0.04 to 0.81; Figure 6). One advantage of the `neonSoilFlux` package is its ability to
393 calculate fluxes across different soil depths (Figure 3), which allows for additional site-specific
394 customization. We believe the package can provide a useful baseline estimate of soil fluxes that
395 can always be complemented through additional field measurements.

396 The six locations studied provide a range of case studies that suggest different considerations
397 may apply to different sites when applying the flux-gradient method. For example, the Santa
398 Rita Experimental Range (SRER) is a desert site characterized by sandy soil, which also was
399 the location of the highest field soil temperatures that we observed (Table 2). At SRER the
400 flux across the top two layers (F_{110}) produced a pattern of soil flux most consistent with the
401 observed field data. The remaining methods F_{101} , F_{011} , or F_{000} are derived from information
402 taken from the deepest layer, which seems to have been decoupled from the surface layers both
403 in terms of temperature and CO₂ concentration. This may be a general circumstance where
404 there are large diurnal temperature extremes that rapidly change during the course of a day
405 and overnight, leading to lags in the timing of when temperature increases propagate down to
406 deeper soil layers.

407 Immediately prior to our visit to Konza Prairie (KONZ), that site that experienced a significant
408 rain event that led to wet soils that gradually dried out over the course of our time there.
409 This pulse of precipitation increased the soil CO₂ concentration at the top layer above the
410 concentrations in lower layers, leading to negative estimated flux values at the start of the field
411 sampling period. In this case it was only when the soil began to return to a baseline level that
412 the assumptions of the flux-gradient method were again met.

413 Both of the previous cases also provide context for the variable statistical comparisons between
414 field-measured soil fluxes and `neonSoilFlux` outputs (Figure 6). When considering systematic
415 deployment of this method across a measurement network, there are a number of independent

416 challenges that require careful consideration. There are clear tradeoffs between (1) accuracy of
417 modeled fluxes (defined here as closeness to field-measured F_S and the uncertainty reduction
418 factor ϵ), (2) precision (which could be defined by the signal to noise ratio), and (3) the
419 choice of the diffusivity model (Section 4.2.2) or flux computation method (Section 4.2.3). A
420 sensitivity analysis (Figure S2, Supplemental Information) found that flux output uncertainty
421 was dominated by measurement uncertainty (T_S , P , SWC , or CO_2) rather than by the
422 diffusivity method used to compute soil flux. Notably, the F_{110} method was least sensitive to
423 measurement uncertainty likely because it best aligns with the surface chamber measurement
424 assumptions.

425 Finally, comparing the effects of different diffusivity estimation methods on the match between
426 modeled and measured fluxes (Figure 5) highlights the sensitivity of F_{ijk} to diffusivity. The
427 comparison between diffusivity estimates compared to field estimated diffusivity (Figure 7)
428 demonstrates that site parameters can dictate which measure of diffusivity is most likely to be
429 accurate in a given environmental context. Site-specific differences are largely a reflection of
430 differences in soil moisture across the sites (Table 1), as not all diffusivity estimation methods
431 incorporate soil moisture equivalently. While we here have compares two approaches to calculate
432 diffusivity (the Millington-Quirk and Marshall models), it may be valuable to evaluate other
433 diffusivity models (e.g. the Moldrup model; Moldrup et al. (1999)) as well. Ultimately the
434 choice of a particular diffusivity model could be determined based on knowledge of site-specific
435 evaluations or a set of these models could be used to generate a model ensemble average as a
436 means to trade precision for a more general approach.

437 **6.3 Recommendations for future method development**

438 The `neonSoilFlux` package provides several approaches to estimate soil flux using the gradient
439 method. We believe these approaches enable the software to be used across a range of site-

⁴⁴⁰ specific assumptions (Maier & Schack-Kirchner, 2014). We note, however, that this choice
⁴⁴¹ can have a determinative approach on the calculated values. Ensemble averaging approaches
⁴⁴² (Elshall et al., 2018; Raftery et al., 2005) may be one way to address this problem if the goal is
⁴⁴³ to calculate fluxes using the same method at a diverse range of different sites. Two other ideas
⁴⁴⁴ would be to apply machine learning algorithms (e.g. random forest) to generate a single flux
⁴⁴⁵ estimate across diverse sites, or using co-located estimates of net ecosystem carbon exchange
⁴⁴⁶ from eddy-flux towers to further constrain results or to assess soil flux results for plausibility
⁴⁴⁷ (Phillips et al., 2017).

⁴⁴⁸ These challenges notwithstanding, the method used here and made available in the
⁴⁴⁹ `neonSoilFlux` R package has the potential to produce nearly continuous estimates of flux
⁴⁵⁰ across all terrestrial NEON sites. These estimates are a significant improvement on available
⁴⁵¹ approaches to constrain the portion of ecosystem respiration attributable to the soil. This, in
⁴⁵² turn, also aids in our ability to understand the soil contribution to the net ecosystem flux
⁴⁵³ measured at these sites using the co-located eddy flux towers.

⁴⁵⁴ 7 Conclusions

⁴⁵⁵ We used the R package `neonSoilFlux` to estimate soil CO₂ fluxes with the flux-gradient method
⁴⁵⁶ using data from buried soil sensors at NEON terrestrial sites. We compared the predicted
⁴⁵⁷ fluxes to those measured directly using a field-based closed chamber approach. Soil fluxes
⁴⁵⁸ from `neonSoilFlux` were broadly effective at producing estimates of flux comparable to those
⁴⁵⁹ measured in the field using a chamber-based technique. However `neonSoilFlux` outputs are
⁴⁶⁰ quite sensitive to a number of issues, including: missing data (and thus gap-filling of input
⁴⁶¹ measurement datasets), the selection of soil depths used to best calculate the gradient (which
⁴⁶² may vary between sites), and finally the choice of method used for estimating soil diffusivity.

463 The flexibility of the `neonSoilFlux` package allows the user to evaluate each of these issues
464 with site-specific knowledge and contexts. Future refinements and subsequent validation of
465 `neonSoilFlux` outputs will feed forward into evaluating soil carbon fluxes broader spatial scales
466 to enhance understanding of the ways in which soils across diverse ecosystems are responding
467 to a changing climate.

468 Sources Cited

- 469 Ayres, E., Reichle, R. H., Colliander, A., Cosh, M. H., & Smith, L. (2024). Validation of
470 Remotely Sensed and Modeled Soil Moisture at Forested and Unforested NEON Sites.
471 *IEEE Journal of Selected Topics in Applied Earth Observations and Remote Sensing*, 17,
472 14248–14264. <https://doi.org/10.1109/JSTARS.2024.3430928>
- 473 Baldocchi, D. (2014). Measuring fluxes of trace gases and energy between ecosystems and the
474 atmosphere - the state and future of the eddy covariance method. *Global Change Biology*,
475 20(12), 3600–3609. <https://doi.org/10.1111/gcb.12649>
- 476 Berenbaum, M. R., Carpenter, S. R., Hampton, S. E., Running, S. W., & Stanzione, D. C.
477 (2015). *Report from the NSF BIO Advisory Committee Subcommittee on NEON Scope
478 Impacts*.
- 479 Bond-Lamberty, B. (2018). New Techniques and Data for Understanding the Global Soil
480 Respiration Flux. *Earth's Future*, 6(9), 1176–1180. <https://doi.org/10.1029/2018EF000866>
- 481 Bond-Lamberty, B., Ballantyne, A., Berryman, E., Fluet-Chouinard, E., Jian, J., Morris, K.
482 A., Rey, A., & Vargas, R. (2024). Twenty Years of Progress, Challenges, and Opportuni-
483 ties in Measuring and Understanding Soil Respiration. *Journal of Geophysical Research:
484 Biogeosciences*, 129(2), e2023JG007637. <https://doi.org/10.1029/2023JG007637>
- 485 Bond-Lamberty, B., Christianson, D. S., Malhotra, A., Pennington, S. C., Sihi, D., AghaK-
486 ouchak, A., Anjileli, H., Altaf Arain, M., Armesto, J. J., Ashraf, S., Ataka, M., Baldocchi,

- 487 D., Andrew Black, T., Buchmann, N., Carbone, M. S., Chang, S.-C., Crill, P., Curtis, P.
488 S., Davidson, E. A., ... Zou, J. (2020). COSORE: A community database for continuous
489 soil respiration and other soil-atmosphere greenhouse gas flux data. *Global Change Biology*,
490 26(12), 7268–7283. <https://doi.org/10.1111/gcb.15353>
- 491 Bond-Lamberty, B., & Thomson, A. (2010). A global database of soil respiration data.
492 *Biogeosciences*, 7(6), 1915–1926. <https://doi.org/10.5194/bg-7-1915-2010>
- 493 Bond-Lamberty, B., Wang, C., & Gower, S. T. (2004). A global relationship between the
494 heterotrophic and autotrophic components of soil respiration? *Global Change Biology*,
495 10(10), 1756–1766. <https://doi.org/10.1111/j.1365-2486.2004.00816.x>
- 496 Bouma, T. J., & Bryla, D. R. (2000). On the assessment of root and soil respiration for soils of
497 different textures: Interactions with soil moisture contents and soil CO₂ concentrations.
498 *Plant and Soil*, 227(1), 215–221. <https://doi.org/10.1023/A:1026502414977>
- 499 Chen, H., & Tian, H.-Q. (2005). Does a General Temperature-Dependent Q10 Model of Soil
500 Respiration Exist at Biome and Global Scale? *Journal of Integrative Plant Biology*, 47(11),
501 1288–1302. <https://doi.org/10.1111/j.1744-7909.2005.00211.x>
- 502 Davidson, E. A., Janssens, I. A., & Luo, Y. (2006). On the variability of respiration in
503 terrestrial ecosystems: Moving beyond Q10. *Global Change Biology*, 12, 154–164. <https://doi.org/10.1111/j.1365-2486.2005.01065.x>
- 505 Desai, A. R., Murphy, B. A., Wiesner, S., Thom, J., Butterworth, B. J., Koupaei-Abyazani, N.,
506 Muttaqin, A., Paleri, S., Talib, A., Turner, J., Mineau, J., Merrelli, A., Stoy, P., & Davis,
507 K. (2022). Drivers of Decadal Carbon Fluxes Across Temperate Ecosystems. *Journal of*
508 *Geophysical Research: Biogeosciences*, 127(12), e2022JG007014. <https://doi.org/10.1029/2022JG007014>
- 510 Efron, B., & Tibshirani, R. J. (1994). *An Introduction to the Bootstrap*. Chapman and
511 Hall/CRC. <https://doi.org/10.1201/9780429246593>
- 512 Elshall, A. S., Ye, M., Pei, Y., Zhang, F., Niu, G.-Y., & Barron-Gafford, G. A. (2018). Relative

- 513 model score: A scoring rule for evaluating ensemble simulations with application to microbial
514 soil respiration modeling. *Stochastic Environmental Research and Risk Assessment*, 32(10),
515 2809–2819. <https://doi.org/10.1007/s00477-018-1592-3>
- 516 Falge, E., Baldocchi, D., Olson, R., Anthoni, P., Aubinet, M., Bernhofer, C., Burba, G.,
517 Ceulemans, R., Clement, R., Dolman, H., Granier, A., Gross, P., Grünwald, T., Hollinger,
518 D., Jensen, N.-O., Katul, G., Keronen, P., Kowalski, A., Lai, C. T., ... Wofsy, S. (2001).
519 Gap filling strategies for defensible annual sums of net ecosystem exchange. *Agricultural
520 and Forest Meteorology*, 107(1), 43–69. [https://doi.org/10.1016/S0168-1923\(00\)00225-2](https://doi.org/10.1016/S0168-1923(00)00225-2)
- 521 Farrance, I., & Frenkel, R. (2012). **Uncertainty of Measurement: A Review of the Rules
522 for Calculating Uncertainty Components through Functional Relationships.** *The Clinical
523 Biochemist Reviews*, 33(2), 49–75.
- 524 Friedlingstein, P., O'Sullivan, M., Jones, M. W., Andrew, R. M., Hauck, J., Landschützer,
525 P., Le Quéré, C., Li, H., Luijkx, I. T., Olsen, A., Peters, G. P., Peters, W., Pongratz, J.,
526 Schwingshackl, C., Sitch, S., Canadell, J. G., Ciais, P., Jackson, R. B., Alin, S. R., ...
527 Zeng, J. (2025). Global Carbon Budget 2024. *Earth System Science Data*, 17(3), 965–1039.
528 <https://doi.org/10.5194/essd-17-965-2025>
- 529 Hamdi, S., Moyano, F., Sall, S., Bernoux, M., & Chevallier, T. (2013). Synthesis analysis
530 of the temperature sensitivity of soil respiration from laboratory studies in relation to
531 incubation methods and soil conditions. *Soil Biology and Biochemistry*, 58, 115–126.
532 <https://doi.org/10.1016/j.soilbio.2012.11.012>
- 533 Jackson, R. B., Lajtha, K., Crow, S. E., Hugelius, G., Kramer, M. G., & Piñeiro, G. (2017).
534 The Ecology of Soil Carbon: Pools, Vulnerabilities, and Biotic and Abiotic Controls.
535 *Annual Review of Ecology, Evolution and Systematics*, 48(Volume 48, 2017), 419–445.
536 <https://doi.org/10.1146/annurev-ecolsys-112414-054234>
- 537 Jian, J., Bailey, V., Dorheim, K., Konings, A. G., Hao, D., Shiklomanov, A. N., Snyder,
538 A., Steele, M., Teramoto, M., Vargas, R., & Bond-Lamberty, B. (2022). Historically

- 539 inconsistent productivity and respiration fluxes in the global terrestrial carbon cycle. *Nature*
540 *Communications*, 13(1), 1733. <https://doi.org/10.1038/s41467-022-29391-5>
- 541 Jian, J., Vargas, R., Anderson-Teixeira, K., Stell, E., Herrmann, V., Horn, M., Kholod, N.,
542 Manzon, J., Marchesi, R., Paredes, D., & Bond-Lamberty, B. (2021). A restructured and
543 updated global soil respiration database (SRDB-V5). *Earth System Science Data*, 13(2),
544 255–267. <https://doi.org/10.5194/essd-13-255-2021>
- 545 Jiang, J., Feng, L., Hu, J., Liu, H., Zhu, C., Chen, B., & Chen, T. (2024). Global soil
546 respiration predictions with associated uncertainties from different spatio-temporal data
547 subsets. *Ecological Informatics*, 82, 102777. <https://doi.org/10.1016/j.ecoinf.2024.102777>
- 548 Jobbágy, E. G., & Jackson, R. B. (2000). The Vertical Distribution of Soil Organic Carbon
549 and its Relation to Climate and Vegetation. *Ecological Applications*, 10(2), 423–436.
550 [https://doi.org/10.1890/1051-0761\(2000\)010%5B0423:TVDOSO%5D2.0.CO;2](https://doi.org/10.1890/1051-0761(2000)010%5B0423:TVDOSO%5D2.0.CO;2)
- 551 Jurasinski, G., Koebisch, F., Guenther, A., & Beetz, S. (2022). *Flux: Flux Rate Calculation*
552 *from Dynamic Closed Chamber Measurements.*
- 553 Liu, K., Li, X., Wang, S., & Zhang, H. (2023). A robust gap-filling approach for European
554 Space Agency Climate Change Initiative (ESA CCI) soil moisture integrating satellite
555 observations, model-driven knowledge, and spatiotemporal machine learning. *Hydrology*
556 and *Earth System Sciences*, 27(2), 577–598. <https://doi.org/10.5194/hess-27-577-2023>
- 557 Lunch, C., Laney, C., Mietkiewicz, N., Sokol, E., Cawley, K., & NEON (National Ecological
558 Observatory Network). (Network), N. (National, E. O. (2025). *neonUtilities: Utilities for*
559 *working Working with NEON dataData.*
- 560 Luo, Y., Ogle, K., Tucker, C., Fei, S., Gao, C., LaDeau, S., Clark, J. S., & Schimel, D. S. (2011).
561 Ecological forecasting and data assimilation in a data-rich era. *Ecological Applications*,
562 21(5), 1429–1442. <https://doi.org/10.1890/09-1275.1>
- 563 Maier, M., & Schack-Kirchner, H. (2014). Using the gradient method to determine soil gas
564 flux: A review. *Agricultural and Forest Meteorology*, 192–193, 78–95. <https://doi.org/10.1>

- 565 016/j.agrformet.2014.03.006
- 566 Mariethoz, G., Linde, N., Jougnot, D., & Rezaee, H. (2015). Feature-preserving interpolation
567 and filtering of environmental time series. *Environmental Modelling & Software*, 72, 71–76.
568 <https://doi.org/10.1016/j.envsoft.2015.07.001>
- 569 Marshall, T. J. (1959). The Diffusion of Gases Through Porous Media. *Journal of Soil Science*,
570 10(1), 79–82. <https://doi.org/10.1111/j.1365-2389.1959.tb00667.x>
- 571 Millington, R. J., & Shearer, R. C. (1971). Diffusion in aggregated porous media. *Soil Science*,
572 111(6), 372–378.
- 573 Moffat, A. M., Papale, D., Reichstein, M., Hollinger, D. Y., Richardson, A. D., Barr, A. G.,
574 Beckstein, C., Braswell, B. H., Churkina, G., Desai, A. R., Falge, E., Gove, J. H., Heimann,
575 M., Hui, D., Jarvis, A. J., Kattge, J., Noormets, A., & Stauch, V. J. (2007). Comprehensive
576 comparison of gap-filling techniques for eddy covariance net carbon fluxes. *Agricultural and
577 Forest Meteorology*, 147(3), 209–232. <https://doi.org/10.1016/j.agrformet.2007.08.011>
- 578 Moldrup, P., Olesen, T., Yamaguchi, T., Schjønning, P., & Rolston, D. E. (1999). Modeling
579 diffusion and reaction in soils: 9. The Buckingham-Burdine-Campbell equation for gas
580 diffusivity in undisturbed soil. *Soil Science*, 164(2), 75.
- 581 National Ecological Observatory Network (NEON)NEON. (2024a). *Barometric pres-*
582 *sure (DP1.00004.001)*. National Ecological Observatory Network (NEON). <https://doi.org/10.48443/RT4V-KZ04>
- 583 National Ecological Observatory Network (NEON)NEON. (2024b). *Soil CO₂ concentration*
584 *(DP1.00095.001)*. National Ecological Observatory Network (NEON). <https://doi.org/10.48443/E7GR-6G94>
- 585 National Ecological Observatory Network (NEON)NEON. (2024c). *Soil physical and chemical*
586 *properties, Megapit (DP1.00096.001)*. National Ecological Observatory Network (NEON).
587 <https://doi.org/10.48443/S6ND-Q840>
- 588 National Ecological Observatory Network (NEON)NEON. (2024d). *Soil tempera-*
589

- 591 *ture (DP1.00041.001)*. National Ecological Observatory Network (NEON). <https://doi.org/10.48443/Q24X-PW21>
- 592 **National Ecological Observatory Network (NEON)**NEON. (2024e). *Soil water content and*
593 *water salinity (DP1.00094.001)*. National Ecological Observatory Network (NEON). <https://doi.org/10.48443/A8VY-Y813>
- 594 Norman, J. M., Kucharik, C. J., Gower, S. T., Baldocchi, D. D., Crill, P. M., Rayment,
595 M., Savage, K., & Striegl, R. G. (1997). A comparison of six methods for measuring
596 soil-surface carbon dioxide fluxes. *Journal of Geophysical Research: Atmospheres*, 102(D24),
597 28771–28777. <https://doi.org/10.1029/97JD01440>
- 598 **Pedersen, A. R. (2024). HMR: Flux Estimation with Static Chamber Data.**
- 599 Phillips, C. L., Bond-Lamberty, B., Desai, A. R., Lavoie, M., Risk, D., Tang, J., Todd-Brown,
600 K., & Vargas, R. (2017). The value of soil respiration measurements for interpreting and
601 modeling terrestrial carbon cycling. *Plant and Soil*, 413(1), 1–25. <https://doi.org/10.1007/s11104-016-3084-x>
- 602 Raftery, A. E., Gneiting, T., Balabdaoui, F., & Polakowski, M. (2005). *Using Bayesian Model*
603 *Averaging to Calibrate Forecast Ensembles*. <https://doi.org/10.1175/MWR2906.1>
- 604 **Rheault, K., Christiansen, J. R., & Larsen, K. S. (2024). goFlux: A user-friendly way to**
605 **calculate GHG fluxes yourself, regardless of user experience.** *Journal of Open Source*
606 *Software*, 9(96), 6393. <https://doi.org/10.21105/joss.06393>
- 607 Sallam, A., Jury, W. A., & Letey, J. (1984). Measurement of Gas Diffusion Coefficient under
608 Relatively Low Air-filled Porosity. *Soil Science Society of America Journal*, 48(1), 3–6.
609 <https://doi.org/10.2136/sssaj1984.03615995004800010001x>
- 610 Shao, J., Zhou, X., Luo, Y., Li, B., Aurela, M., Billesbach, D., Blanken, P. D., Bracho, R.,
611 Chen, J., Fischer, M., Fu, Y., Gu, L., Han, S., He, Y., Kolb, T., Li, Y., Nagy, Z., Niu, S.,
612 Oechel, W. C., ... Zhang, J. (2015). Biotic and climatic controls on interannual variability
613 in carbon fluxes across terrestrial ecosystems. *Agricultural and Forest Meteorology*, 205,

- 617 11–22. <https://doi.org/10.1016/j.agrformet.2015.02.007>
- 618 Shao, P., Zeng, X., Moore, D. J. P., & Zeng, X. (2013). Soil microbial respiration from
619 observations and Earth System Models. *Environmental Research Letters*, 8(3), 034034.
620 <https://doi.org/10.1088/1748-9326/8/3/034034>
- 621 Sihi, D., Gerber, S., Inglett, P. W., & Inglett, K. S. (2016). Comparing models of microbial–
622 substrate interactions and their response to warming. *Biogeosciences*, 13(6), 1733–1752.
623 <https://doi.org/10.5194/bg-13-1733-2016>
- 624 Tang, J., Baldocchi, D. D., Qi, Y., & Xu, L. (2003). Assessing soil CO₂ efflux using continuous
625 measurements of CO₂ profiles in soils with small solid-state sensors. *Agricultural and Forest
626 Meteorology*, 118(3), 207–220. [https://doi.org/10.1016/S0168-1923\(03\)00112-6](https://doi.org/10.1016/S0168-1923(03)00112-6)
- 627 Tang, J., Misson, L., Gershenson, A., Cheng, W., & Goldstein, A. H. (2005). Continuous
628 measurements of soil respiration with and without roots in a ponderosa pine plantation
629 in the Sierra Nevada Mountains. *Agricultural and Forest Meteorology*, 132(3), 212–227.
630 <https://doi.org/10.1016/j.agrformet.2005.07.011>
- 631 Taylor, J. R. (2022). *An Introduction to Error Analysis: The Study of Uncertainties in Physical
632 Measurements, Third Edition* (3rd ed.). University Science Press.
- 633 Wilson, S. J., Bond-Lamberty, B., Noyce, G., Bittencourt Peixoto, R., & Megonigal, J. P.
634 (2024). Fluxfinder: An R Package for Reproducible Calculation and Initial Processing
635 of Greenhouse Gas Fluxes From Static Chamber Measurements. *Journal of Geophysical
636 Research: Biogeosciences*, 129(11), e2024JG008208. [https://doi.org/10.1029/2024JG008208
637 08](https://doi.org/10.1029/2024JG008208)
- 638 Yan, Z., Bond-Lamberty, B., Todd-Brown, K. E., Bailey, V. L., Li, S., Liu, C., & Liu, C. (2018).
639 A moisture function of soil heterotrophic respiration that incorporates microscale processes.
640 *Nature Communications*, 9(1), 2562. <https://doi.org/10.1038/s41467-018-04971-6>
- 641 Yan, Z., Liu, C., Todd-Brown, K. E., Liu, Y., Bond-Lamberty, B., & Bailey, V. L. (2016).
642 Pore-scale investigation on the response of heterotrophic respiration to moisture conditions

- 643 in heterogeneous soils. *Biogeochemistry*, 131(1), 121–134. <https://doi.org/10.1007/s10533-016-0270-0>
- 645 Zhang, R., Kim, S., Kim, H., Fang, B., Sharma, A., & Lakshmi, V. (2023). Temporal Gap-Filling
646 of 12-Hourly SMAP Soil Moisture Over the CONUS Using Water Balance Budgeting. *Water
647 Resources Research*, 59(12), e2023WR034457. <https://doi.org/10.1029/2023WR034457>
- 648 Zhao, J. (2019). FluxCalR: A R package for calculating CO₂ and CH₄ fluxes from static
649 chambers. *Journal of Open Source Software*, 4(43), 1751. <https://doi.org/10.21105/joss.01751>
- 650 Zobitz, J., Ayres, E., O'Rourke, K., Werbin, Z., Lee, L., Abdi, R., Mehmeti, D., & Xiong, L.
651 (2024). *neonSoilFlux: Compute Soil Carbon Fluxes for the National Ecological Observatory
652 Network Sites*.